Electroporation

2

Mohammad Hjouj and Boris Rubinsky

Abstract

Nonthermal irreversible electroporation (NTIRE) is a minimally invasive tissue ablation modality in which high field strength, nanosecond to millisecond long pulsed electric fields are delivered across the cell to produce nanoscale defects in the cell membrane and thereby induce cell death. An important attribute of this technique is its ability to ablate cells in volumes of tissues while leaving intact the extracellular scaffold, including the mechanical scaffold of blood vessels and ducts. This is a review of the technology with a special emphasis on medical imaging. The review contains a background on the technology, mathematical modeling for treatment planning, fundamental findings from animal studies, first clinical results, and aspects of medical imaging.

Introduction

Electroporation is an electric field-induced biophysical phenomenon in which the cell membrane permeability to transmembrane molecular transport is increased by exposing the cell to short nanosecond to millisecond scale and high field, kV/cm scale, electric pulses [1, 2]. Such increase in permeability [3] is, presumably [4], related to the formation of nanoscale defects or pores in the cell membrane, from which the term electro-"poration" [5] stems. For certain electric pulses, membrane permeabilization is permanent, and the process leads to cell lysis. It is in this sense of permanent permeabilization that most authors define irreversible electroporation (IRE). However, it must be noted that temporary permeabilization can also cause a severe disruption of the cell homeostasis which can finally result in cell death, either necrotic or apoptotic. Therefore, in a broader sense, IRE could be defined as the permanent or temporal membrane electroporation process that causes cells to die.

The phenomenon of irreversible electroporation – cell death due to the applications of short electric pulses – has been recognized, in various forms, for centuries and until

M. Hjouj (✉)
School of Computer Science and Engineering, Hebrew University of Jerusalem, Jerusalem, Israel

Department of Medical Imaging, Al–Quds University, Abu–Dis, Palestine
e-mail: mhjouj@hotmail.com

B. Rubinsky
Department of Mechanical Engineering, University of California at Berkeley, Berkeley, CA, USA
e-mail: rubinsky@me.berkeley.edu; brubinsky@gmail.com

D.E. Dupuy et al. (eds.), *Image-Guided Cancer Therapy*, DOI 10.1007/978-1-4419-0751-6_4,

recently used primarily in the food industry [6]. The biophysical phenomenon referred in medical applications as "irreversible electroporation" is known in food technology as *pulsed electric field* processing or *electroplasmolysis*, in reference to the lysis of cell membranes in tissue, for extracting their contents, or the bactericidal effect in treatment of fluids [7]. The "pulsed electrical field" concept is broader than just irreversible electroporation. It has been recently shown to include also the effects of nanoscale pulses on intracellular components [8]. The interest of the food industry in the so-called bactericidal action of electrical fields motivated a series of three seminal papers by Sale and Hamilton [9–11]. These papers are extraordinary in that they set the basis for the field of irreversible electroporation and contain the ingredients of many of the future studies in what subsequently was called the field of electroporation in general.

Recently, nonthermal irreversible electroporation (NTIRE) has begun to be employed as a new tool in the surgical armamentarium for minimally invasive ablation of undesirable tissue [12]. In NTIRE, the primary use of irreversible electroporation is to induce undesirable cell death by affecting selectively only the cell membrane without causing a possible thermal mode of damage due to excessive electric current-induced Joule heating. Specifically, care is given to choosing electric pulse parameters that induce irreversible electroporation without causing thermal damage [13, 14]. The research in the field of nonthermal irreversible electroporation in medicine has recognized that while the final outcome of irreversible electroporation and thermal damage on cell viability is the same, cell death, there are many very important aspects at the microscale which are different. Unlike electroporation that affects only one type of molecule in the treated volume – the cell membrane lipid bilayer – thermal, radiation, as well as chemical (alcohol) ablation indiscriminately affect every molecule in the treated volume. Therefore, when a volume of tissue is ablated by irreversible electroporation only, the procedure has molecular selectivity (i.e., it targets one type of molecule only, the cell membrane lipid bilayer). Having a minimally invasive technique that can ablate only one certain type of molecule, the cell membrane, is advantageous – because it spares important other tissue components such as the extracellular matrix and electrically nonconductive molecular structures. An intact extracellular matrix after NTIRE treatment allows such structures as ducts, large blood vessels, or nerve conduits to continue to serve their physical function, even in the absence of cells. This facilitates the treatment of tumors that abut large blood vessels in previously inaccessible parts and organs of the body such as the pancreas [15, 16], near large blood vessels in the liver [17–19], and kidney [20]. Retaining the patency of the large blood vessels also facilitates a much faster response of the immune system and sometimes healing without the formation of scar tissue [21]. It was also shown that the selectivity of NTIRE can lead to survival and regeneration of nerves [22–24]. The intact extracellular matrix can also serve as a template for cell regeneration after NTIRE. For instance, Maor and colleagues have shown that the carotid artery continues to serve as an effective blood conduit after NTIRE [25, 26]. Furthermore, endothelial cells regenerate and grow along the NTIRE-treated blood vessel on the intact extracellular matrix [25, 26].

Typical NTIRE procedures employ two or more electrodes inserted in tissue in such a way as to confine the undesirable tissues between them [21]. The electrodes can be mounted on one probe (e.g., [25–27]) or on several probes (Fig. 2.1) [21]. The process of tissue ablation occurs between electrodes and is usually confined by the electrodes (Fig. 2.2). In this respect, NTIRE is different from most of the other ablation techniques in which the ablation propagates as a function of time from the probe outward. NTIRE is also different from other minimally invasive tissue ablation techniques by the time scale in which the procedure occurs. The electric pulses that induce NTIRE are on the length scale of nanosecond to milliseconds. NTIRE is delivered as a set of pulses rather than continuously. Current clinical practice employs between 8 and 90 pulses of 70–100 μs length, delivered at a frequency of 1 Hz [17, 19, 28]. In contrast,

Fig. 2.1 Two NTIRE copper, 1 mm diameter, electrodes (*bright lines*) inserted into a pig liver (Courtesy Dr. Stephen Solomon, *Memorial Sloan-Kettering Cancer Center*)

thermal ablation procedures employ time scales from minutes to tens of minutes. Because NTIRE is conceptually different from other more established tissue ablation procedures, such as cryosurgery, radiofrequency ablation, or radiation, it is important for those with experience in the other techniques to understand the particular attributes of NTIRE and how it is different from the other tissue ablation techniques.

We will introduce next the mathematical modeling required for treatment planning of NTIRE. Treatment planning, which is important in every minimally invasive tissue ablation procedure, is essential for correct use of NTIRE. This is followed by a description of fundamental experimental results of NTIRE and a brief survey of clinical results produced so far. Lastly, we will discuss medical imaging of NTIRE with respect to two key aspects: placement of electrodes and procedural follow-up.

Mathematical Models for Nonthermal Irreversible Electroporation

As with other minimally invasive tissue ablation techniques, treatment planning is of great importance and can benefit from mathematical modeling. NTIRE treatment planning mathematical modeling requires the solution of the electric field equation to determine the electric field produced during the procedure. In addition to the field equation in order to avoid thermal damage, the bio-heat equation coupled with a kinetic equation is solved to evaluate if thermal damage occurs [13, 14, 29–32]. In this section, we will first present the set of equations used in NTIRE treatment planning. This is followed by some illustrative examples.

The electric field equation is,

$$\nabla \cdot (\sigma \nabla \phi) = 0 \tag{2.1}$$

subject to voltage boundary conditions on the electrodes:

$$\phi(electrodes) = prescribed \tag{2.2}$$

where σ is the electrical conductivity of the tissue and ϕ is the local electrical potential. It should be emphasized that the electrical conductivity of the tissue can change during the process of electroporation, and therefore the problem may become nonlinear as the local conductivity may become related to the local electrical field. In addition, the boundary conditions prescribed here are of the first kind. It is possible that contact impedance between the electrodes and the tissue may be a more appropriate boundary, e.g., Somersalo et al. [33]. The boundaries of the domain that are not in contact with the electrodes are treated as either infinite or insulated.

The local electrical field, E, can be calculated from the electrical potential:

$$E = \nabla \phi \tag{2.3}$$

This electrical field affects the local conductivity through electroporation effects and makes the problem nonlinear. In addition, it yields a local heat source, P, through Joule heating. The local electrical power dissipation is given by:

$$P = \sigma(|\nabla \phi|)^2 \tag{2.4}$$

The equation most commonly used to calculate the temperature during electroporation in

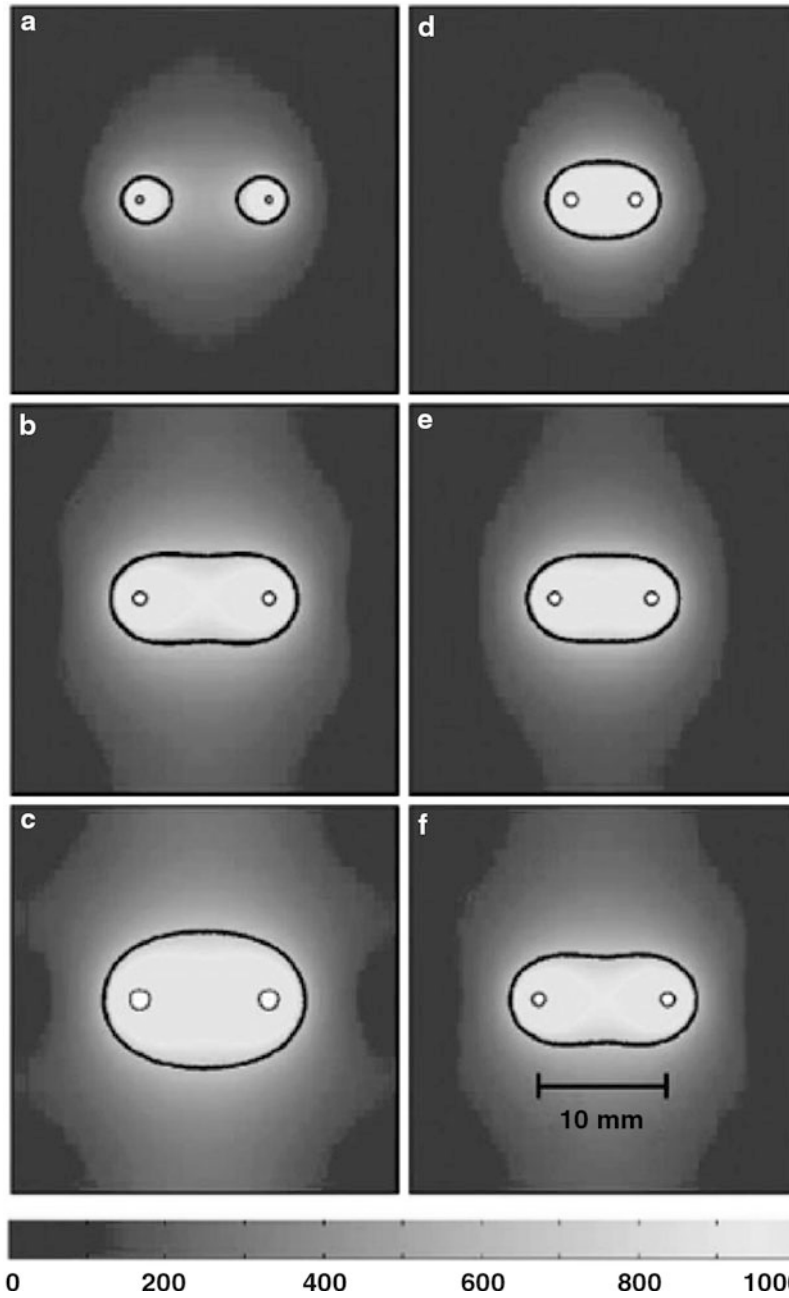

Fig. 2.2 Typical NTIRE ablation zone shapes that can be obtained with two electrodes. The *dark line* shows the interface between the areas that was irreversible electroporated and that was reversible electroporated. The elliptic shape is typical to the treated region, when the electroporation is induced by two electrodes. The lighter area beyond the *dark line* illustrates the reversible electroporated domain. This area may become important in the future uses of reversible electroporation as it allows the incorporation of drugs or genes around the area treated with NTIRE, in the mode of electrochemotherapy (Modified with permission from Ref. [13])

biological tissues is the bio-heat equation [34] to which the local power dissipation is added as a heat source:

$$\nabla \cdot (k\nabla T) + w_b c_b (T_a - T) + q'' + P = \rho c_p \frac{\partial T}{\partial t} \tag{2.5}$$

where k is the thermal conductivity of the tissue, T is temperature, $w_b c_b$ are the product of the volumetric mass flow of blood and blood heat capacity, q'' is the volumetric metabolic heat, t is time, and ρc_p is the product of tissue density and heat capacity of tissue.

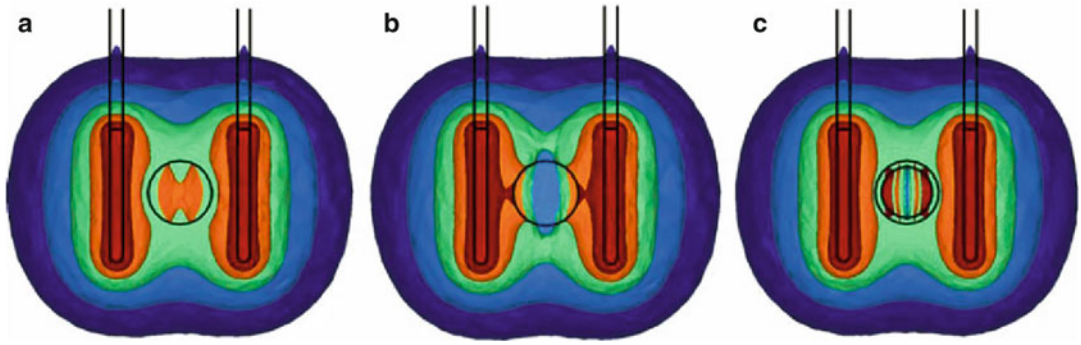

Fig. 2.3 Effect of a heterogeneous tissue conductivity on the electric field distribution. Each graph depicts the surfaces of constant electric field strength (for 100, 200, 400, 800, and 1,600 V/cm) that would result from the presence of a 5-mm-diameter spherical inclusion, located halfway between the electrodes. The inclusion is composed of tissue with one fifth or five times the background electrical conductivity in graphs (**a**) and (**b**), respectively, while (**c**) the third graph is similar to (**a**) but with a nested 4-mm-diameter sphere of five times normal conductivity (With permission from Ref. [32])

This equation is solved subject to initial temperature conditions, which in case of the living body is often taken as 37 °C. The boundary conditions are taken as either 37 °C or adiabatic (no heat transfer occurs). A review of various models of the bio-heat equation can be found in [35].

Once the time-dependent temperature is calculated, it can be introduced into an Arrhenius type of chemical reaction kinetics equation that correlates tissue damage, Ω, to temperature, T, and time, t [36]

$$\Omega = \int \zeta e^{-E/RT} dt \tag{2.6}$$

where ζ is a frequency factor, E is the activation energy, and R is the universal gas constant. It should be emphasized that the thermal damage is a function of both time and temperature and long-term exposure to temperatures as low as 42 °C can cause thermal damage. Nevertheless, when the exposure time is on the order of magnitude of seconds, 50 °C is sometimes taken as a target temperature [37].

Figure 2.2 illustrates typical NTIRE ablation zone shapes that can be obtained with two electrodes [13]. Studies on the treated region shapes that can be obtained with various electrode configurations are found in several publications [13, 14, 29, 32]. It is particularly interesting to note that under certain parameters, the treatment can be incomplete and a zone of untreated tissue can occur between the electrodes (Fig. 2.2a). The lighter area beyond the dark line illustrates the reversible electroporated domain. This area may become important in the future uses of reversible electroporation as it allows the incorporation of drugs or genes around the area treated with NTIRE, in the mode of electrochemotherapy.

Heterogeneities, for instance, a metal clip in the treated area, can affect the treated zone as illustrated in Fig. 2.3 [30, 32]. It is important to understand that in NTIRE, as in other ablation methods, the shape of the electrodes, the placement of the electrodes, and the voltages set on the electrodes will all affect the outcome of the procedure.

Experimental and First Clinical Results of Nonthermal Irreversible Electroporation

This section will highlight first the unique aspects of nonthermal irreversible electroporation, which can be directly attributed to the unique "molecular selective" mode of this procedure. Figure 2.4 is from the first animal study of NTIRE [31] and the results are typical of all the later studies as well. In the study, a rat liver was exposed to a 20-ms NTIRE pulse, and the rat was killed a couple of hours later. The liver

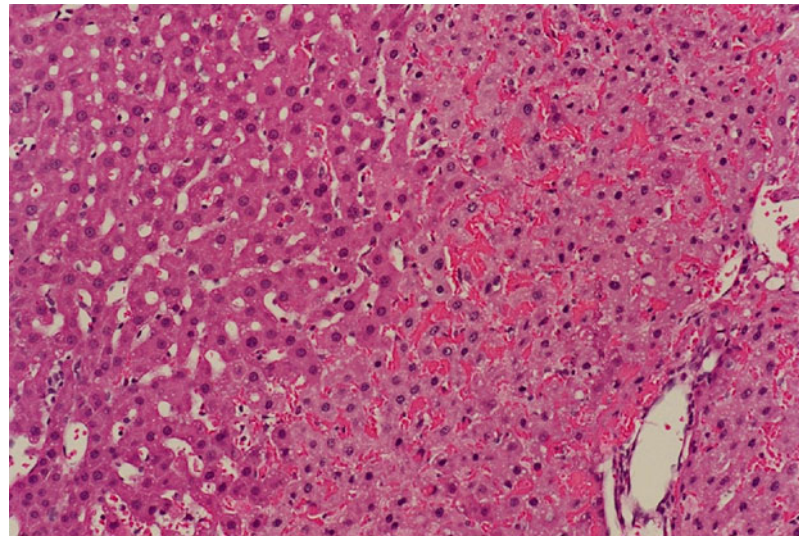

Fig. 2.4 H&E stained liver that has undergone NTIRE. The left-hand side is the normal liver, and the right-hand side is the electroporated liver. Note the sharp line of distinction between the treated and untreated areas. Red blood cells are destroyed and occlude the sinusoids on the right hand while they are open on the left. However, the large blood vessel in the treated area has remained morphologically intact. The *right panels* show an intact vein

was flushed through its vasculature prior to embedding and H&E staining.

Figure 2.4 shows the margin of the NTIRE-treated liver. The light spaces between cells on the left side are the intact sinusoids that were flushed of red blood cells. The hepatocytes around the intact sinusoids are also intact. On the other hand, on the right-hand side, the sinusoids are filled with destroyed red blood cells and other cellular debris. Flushing did not remove the debris from the sinusoids. However, as predicted for the NTIRE mode, the procedure did not affect the extracellular matrix and other tissue molecules, except the cell membrane. Therefore, the mechanical integrity of large blood vessels remains intact. The patency of the large blood vessels and ducts is evident from the bottom right-hand side images of clear large blood vessels in the midst of the NTIRE-treated region. Because of the unique aspects of NTIRE, the mechanical structure of these blood vessels remained intact and accessible to flushing.

The results from the first chronic study of NTIRE in a large animal model are shown in Fig. 2.5, and they are also typical of all the subsequent findings [21].

Figure 2.5 shows a pig liver treated with NTIRE and also flushed prior to embedding in formalin. The top and bottom rows show the macroscopic and H&E stained cross section of the liver at various times after the procedure. The treated areas are outlined. A most unusual aspect of NTIRE, relative to other minimally ablation surgical modalities, which is also being confirmed in clinical studies [19], is how fast the treated liver regenerates. It is particularly interesting to see in the second and third columns that NTIRE can ablate tissue all the way to the margin of the larger blood vessels – an aspect of tissue ablation of great importance in treating of unresectable tumors near large blood vessels [19] and in the pancreas [15, 16]. As in the case of the flushed rat liver, the flushed pig liver had also patent and open large blood vessels within the treated area. Such open and mechanically intact large blood vessels do not occur during thermal treatment with radio frequency, focused ultrasound, or microwave. The availability of such open conduits allows the immune system excellent access to all the parts of the treated tumor tissue, through the blood flow. In other modes of ablation – the immune system needs to remove the dead cells by diffusion through the volume of treated tissue from the outer margin of the treated tissue. In NTIRE, the entire volume of the treated tissue is accessible through the large blood vessels, and the immune system can remove the dead cells through the entire treated system. This effect is evident from the bottom row of Fig. 2.5, which shows the lymph nodes.

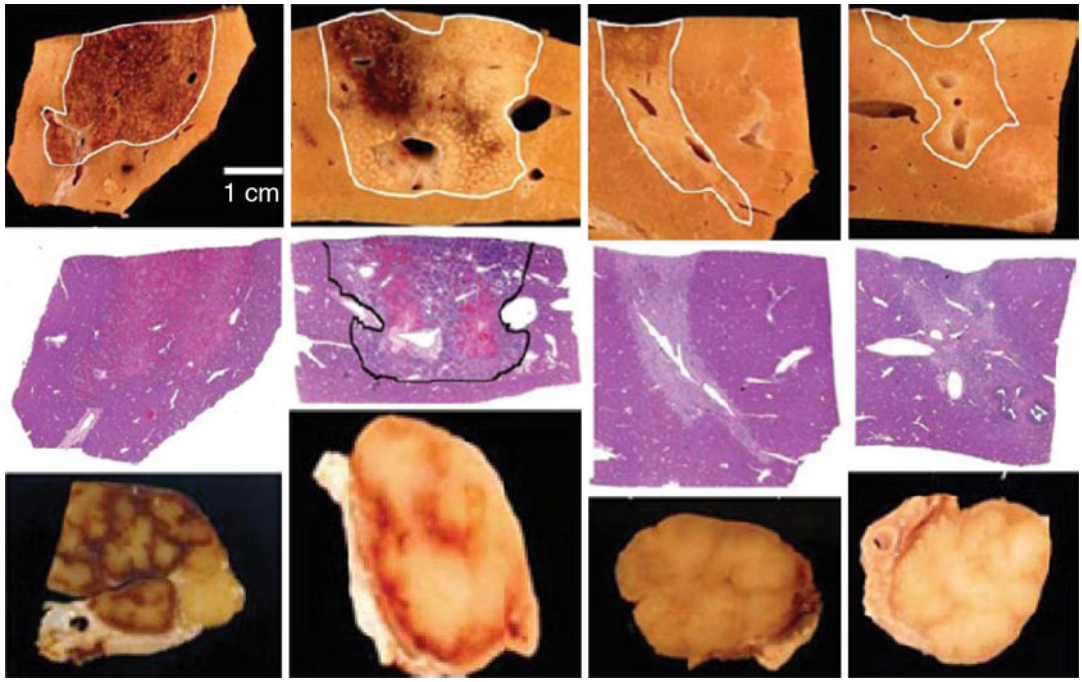

Fig. 2.5 Cross section through NTIRE-treated pig liver after 24 h (first column from *left*), 3 days (second column), 7 days (third column), 14 days (fourth column). *Top row* – macroscopic cross section: *middle row* – H&E stained section: *bottom row* – lymph nodes (Reprinted from Ref. [21])

It is evident that after 24 h, the lymph nodes are inflamed and active. However, within a week, the inflammation has disappeared.

Figure 2.6 shows that bile ducts as well as arteries remain intact in the NTIRE-treated volume of tissue.

At the time this review is written, NTIRE has been already used to treat a variety of malignant tumors including, liver, kidney, lymph nodes, lung, and prostate in well over 800 patients. However, very few scientific reports have been published so far. Nevertheless, published clinical studies [17, 19, 28, 38, 39] produce observations that are consistent with the results from animal experiments.

Brausi et al. confirmed the safety of NTIRE in treatment of prostate cancer [28]. The clinical work of Onik [38] in the prostate confirmed many of the advantages seen in the animal studies treated using NTIRE. In terms of tissue destruction, animal studies showed that IRE lesions are characterized by uniform necrosis throughout, with a very narrow zone of transition to

Fig. 2.6 Intact bile ducts and arteries within NTIRE-treated tissue

unaffected tissue. Two postoperative biopsies in patients showed complete epithelial cell ablation in all the cores taken from all patients. No viable glandular elements were identified, although ghosts of glandular structures were still identifiable. Of interest is that these results were independent of Gleason score with successful

treatment of patients with Gleason score of seven and eight. Despite the uniform destruction of glandular cellular elements evidenced in biopsies, sparing of normal structures was also demonstrated. Post-op pathology and color Doppler US demonstrated intact and functioning micro- and macrovasculature, particularly in the prostate neurovascular bundle. This characteristic appears to be unique to NTIRE lesions. While IRE does cause endothelial cell death, it does not cause vessel occlusion. Also noted on the biopsies was the preservation of nerves and ganglion cells within the NTIRE lesions despite them being included in the NTIRE lesion. All the patients who were potent prior to treatment were immediately potent after treatment, while it did take approximately 6 months for two patients who were treated bilaterally to regain their potency. A number of patients were successfully treated despite tumors being adjacent to the urethra. Of note is that two of the patients were also radiation failures. In one of the patients, the tumor involved the midline ejaculatory duct region. Despite very aggressive treatment in this area, the patient's ejaculatory ducts remained intact, allowing for normal ejaculation postoperatively. This is unique to IRE ablation. Nevertheless, animal studies suggest a need for cautions. IRE will ablate both smooth and striated muscle. Although all patients in this initial experience were continent immediately, care still needs to be taken not to destroy both the internal and external sphincter which would result in incontinence because NTIRE can ablate muscle cells. From a technical point of view, NTIRE is similar to other transperineal ultrasound-guided procedures such as cryosurgery and brachytherapy. However, it is important to emphasize that general anesthesia with patient paralysis is needed due to the muscle contraction associated with the electrical pulsing. The speed of the IRE procedure is however impressive compared to cryoablation and HIFU. The multiple pulses for the treatment are delivered in a few minutes rather than the much longer process of freezing and thawing associated with cryoablation or the numerous small ablation zones necessary in HIFU. The Albert Hospital group of Dr. Kenneth Thomson has produced by far, the majority of peer reviewed reports on clinical use of NTIRE [17, 19, 39]. They have used general anesthesia with muscular paralysis to ensure that the energy applied to the electrodes did not cause severe muscle contraction. Even with the patient fully paralyzed, the energy delivered by the IRE is sufficient to cause contraction of a muscle in the immediate vicinity of the electrodes. Additional patient monitoring using BIS monitors and a direct arterial pressure monitor was used as during the application of the electroporation, the electrocardiogram tracing was significantly distorted by the electrical energy. In a few patients, the electrical energy generated extra systoles and in one patient, a series of contractions which did not provide adequate cardiac output for several seconds. As a result of these cardiac arrhythmias, an ECG synchronizing device was used to deliver the IRE energy 50 μs following the peak of the R wave. While this device prevented the arrhythmias, the delivery of the energy was markedly delayed as in most patients, only one or two pulses could be delivered per heartbeat. In practice however, the time of delivery of the energy is not a rate-limiting factor.

Thomson reports that "The promise of preservation of the structural integrity of the tissue was achieved and as a result of this we have been able to place the electrodes in an extremely aggressive manner with respect to vital organs. Where a tumor lies adjacent to a large bile duct, blood vessel or other vital structure, with imaging guidance it is a simple matter to position the electrodes in such a way as not to puncture the vessel or structure yet provide a zone of electroporation which involves the region of the vessel structure. Likewise lesions adjacent to the gall bladder, stomach, diaphragm and right atrium have been accessed effectively without evidence of damage to these adjacent vital structures…The most remarkable feature of recovery following irreversible electroporation… is the almost complete absence of post-ablation pain. In this group of patients who have been subjected to most other alternatives including chemotherapy, surgery and thermal ablation, this feature of (IRE) is most remarkable. From a histological point of view,

tissue biopsies taken one month after the procedure demonstrated 'coagulate necrosis' with preservation of tissue structure. On CT follow-up at periods between 1 and 8 months, there has been no evidence of residual damage to blood vessels or bile ducts. Since the biliary endothelium would have suffered the same fate as the tumor cells with electroporation, it is surprising that we have not seen evidence of bile duct stricture. Vascular endothelium and smooth muscle should also be ablated with irreversible electroporation but we have not been able to detect any deleterious effect to blood vessels in our patients." In a follow-up study, Ball et al. [19] conclude that "Relaxant general anesthesia is required for IRE of the liver, lung, and kidney. An electrocardiogram synchronizer should be used to minimize the risk of arrhythmias. Attention to the position of the arms is required to maximize CT scan quality but minimize brachial plexus strain. Simple postoperative analgesia is all that is required in most patients."

The group of Davalos produced a recent series of reports on clinical use of NTIRE in dogs with tumors in their brain. The results are very promising showing that, e.g., the procedure can successfully treat a large sarcoma [40].

Medical Imaging in Nonthermal Irreversible Electroporation

Similar to other minimally invasive tissue ablation techniques, IRE is also dependent on two important aspects of medical imaging. The first is placement of the IRE probes (electrodes), and the second is imaging the outcome of the procedure. Unlike thermal tissue ablation modalities such as cryosurgery or radiofrequency, IRE requires the use of two electrodes and not only one enabling probe. In IRE, the two electrodes bound the tissue that is ablated, and the ablation is virtually instantaneous. In the thermal modalities, the tissue ablation process propagates as a function of time from the thermal probe outward. This affects the mode of placing the probes. In IRE, the probe needs to be placed in such a way that the tissue to be ablated is between the

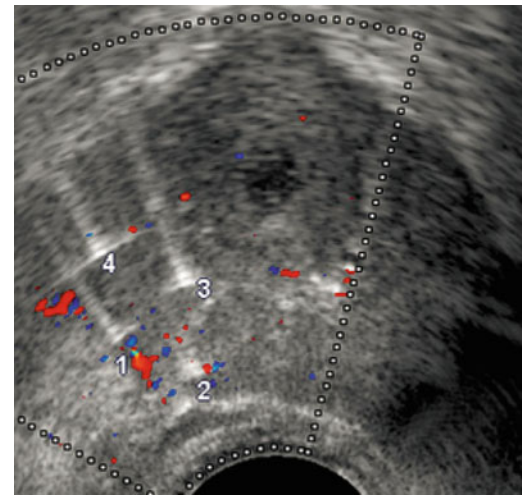

Fig. 2.7 Ultrasound showing the IRE probes (*bright numbered points*) in a parallelogram pattern bracing the area of the know tumor (With permission from Ref. [38])

electrodes, i.e., they are at the periphery of the tissue to be ablated. In contrast, in thermal ablation, the probes are placed in the core of the tissue that needs to be ablated so that the ablation propagates in time from the core to the periphery. Placement of the probes is done with imaging (as shown in Fig. 2.1).

Oni [38] reports that in the prostate procedure, patients were placed in the dorsal lithotomy position, and 18-gauge IRE electrodes were placed under transrectal ultrasound guidance percutaneously through the perineum. IRE probes were placed to cover the known area of cancer location based on the patients mapping biopsy. Four probes were placed in a roughly square array, 1–1.5 cm apart, with the known area of cancer in the center of the array (Fig. 2.7).

Thomson [17, 19, 39] reports that in his experience, in humans, especially in the case of metastases from colorectal carcinoma, ultrasound visualization solutions were difficult, and therefore, computed tomography was used for image guidance. This was even more necessary in the lungs and in most of the renal tumors that were treated (Fig. 2.8).

The other complicating factor in the group of patients chosen for treatment was the inability to reliably place a grid pattern of electrodes

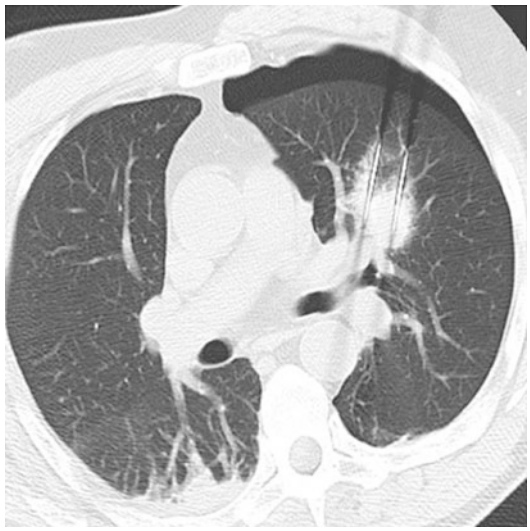

Fig. 2.8 Solitary hilar metastasis with electrodes in position astride the *upper pole* pulmonary artery. No hemoptysis after the IRE procedure. Pneumothorax resolved on drainage in 24 h (From Ref. [39] with permission, Reprinted with permission from Thomson [22])

over the tumor. This was because of the overlying ribs, scapula, and other vital organs. "Unlike the prostate, where a rectangular grid could be used to accurately space the electrodes throughout the gland, in the liver, the spacing of the electrodes was usually performed in an oblique manner from a limited access point in the intercostal space. This aspect of the treatment remains the most difficult in terms of planning and execution. As our experience has grown, we have moved from planning a "slab-to-slab" delivery to planning a "point-to-point" delivery of electroporation. We have also reduced the electrode exposure from 40 to 20–30 mm" [19]. Thomson, as well as Onik, found that positioning the electrodes through the tumor mass remains the most time-consuming facet of the procedure. Anecdotal reports from other physicians performing NTIRE confirm this observation. Placement of the electrodes under imaging is the part of the procedure which is most prone to mistakes and requires radiology skills from the interventional physicians. Since the distance between the electrodes is of importance, when the probes are not within the allowed distance, untreated regions can occur between the electrodes as in (Fig. 2.2a). Thomson [39] reports that early in their experience, this scenario resulted in what he terms "skip lesions" as the entire tumor had not been completely electroporated. This further illustrates the challenges facing the physicians using imaging to place the multiple electrodes for ablation. Developing imaging-assisted skills for optimal probe placement is an important area of clinical research, whose successful completion will substantially improve the outcome of NTIRE.

Perhaps one of the most important advances in minimally invasive surgery was made when imaging was first used to detect the extent of freezing during cryosurgery [41, 42]. Although in cryosurgery the extent of freezing is not equivalent to the extent of tissue ablation, it nevertheless provides a measure of control over the procedure. Therefore, we tried to determine, early in developing IRE, if the outcome of the procedure can be visualized with imaging modalities. Most interesting was the finding that immediately following pulse application ultrasound showed a markedly hypoechoic lesion in the expected location of the IRE lesion [Fig. 2.9b (axial) and Fig. 2.9c (sagittal)] [21]. At 24 h, the ultrasound image showed the hypoechoic lesion had changed character and was now uniformly hyperechoic [21].

Histology as well as mathematical modeling of treatment planning has shown that the hypoechoic lesion seen immediately after NTIRE on ultrasound corresponds well with the region of predicted and measured tissue ablation (Fig. 2.10) [21]. Similar observations on ultrasound imaging of IRE were reported by Lee et al. [43]. Thomson [17, 19, 39] also reports that in those patients in whom ultrasound could be used, similar findings were observed in terms of immediate loss of ultrasound echogenicity with electroporation. While the mechanism which gives rise to the image is not certain, it is most possible related to the destruction of the red blood cells in the small blood vessels. This would be more pronounced in vascular organs as the liver, although it was also observed in the kidney and to a lesser degree in the prostate. Thomson [39] has found that computer tomography (CT)

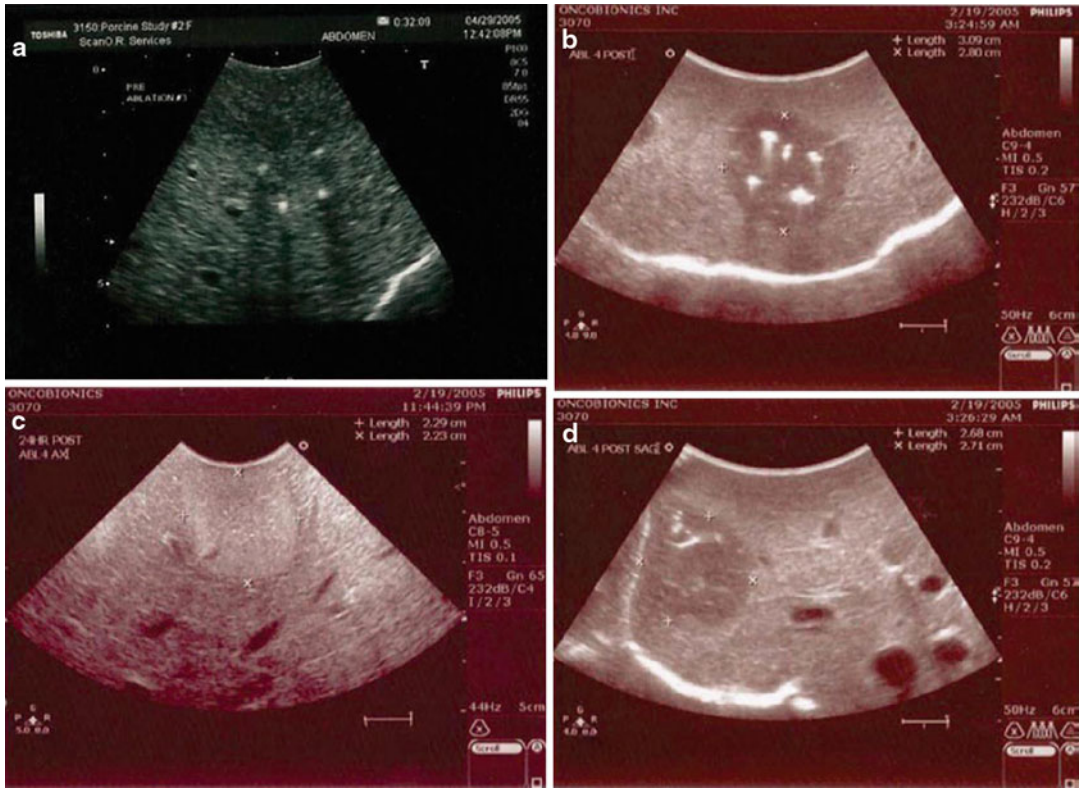

Fig. 2.9 Ultrasound imaging of IRE ablation in the pig liver. (**a**) The placement of the electroporation probes under ultrasound, *hyperechoic dots* represents the electroporation needles. (**b**) Shows axial ultrasound with four hyperechoic dots representing the four needles tracks. The hypoechoic appearance of the expected area of the IRE lesion is noted. (**c**) Sagittal view of the same lesion. The hypoechoic appearance of the expected area of the IRE lesion is noted. (**d**) Sagittal view of the treated area taken 24 h post-IRE. Lesion has now become hyperechoic. Seems to have shrunk by about 4–5 mm. Scale bar 1 cm (From Ref. [21] with permission)

also produces similar images of NTIRE (Fig. 2.11). The group of Kee et al. [18] has also shown that essentially every imaging modality (e.g., MRI, CT, and ultrasound) produces images of the NTIRE-treated areas.

In two recent papers [44, 45], the group of Larson has investigated the use of MRI, with and without contrast material, in a rodent animal model to detect the extent of the treated tissue regions after irreversible electroporation (IRE). Using MR imaging compatible electrodes, the IRE procedure was imaged with T1- and T2-weighted images acquired before and immediately after application of the IRE pulses. MR imaging measurements were compared with both finite element modeling (FEM)-anticipated ablation zones and histologically confirmed ablation zones at necropsy. MR imaging measurements permitted immediate depiction of IRE ablation zones that were hypointense on T1-weighted images and hyperintense on T2-weighted images. MR imaging-based measurements demonstrated excellent consistency with FEM-anticipated ablation zones (for both T1- and T2-weighted images). MR imaging measurements were also highly correlated with histologically confirmed ablation zone measurements. In the contrast material-enhanced magnetic resonance (MR) imaging study, IRE was monitored with conventional T1-weighted gradient-recalled echo (GRE) and inversion recovery (IR)-prepared GRE methods to quantitatively measure the size of irreversible electroporation. IRE ablation zones were produced by using

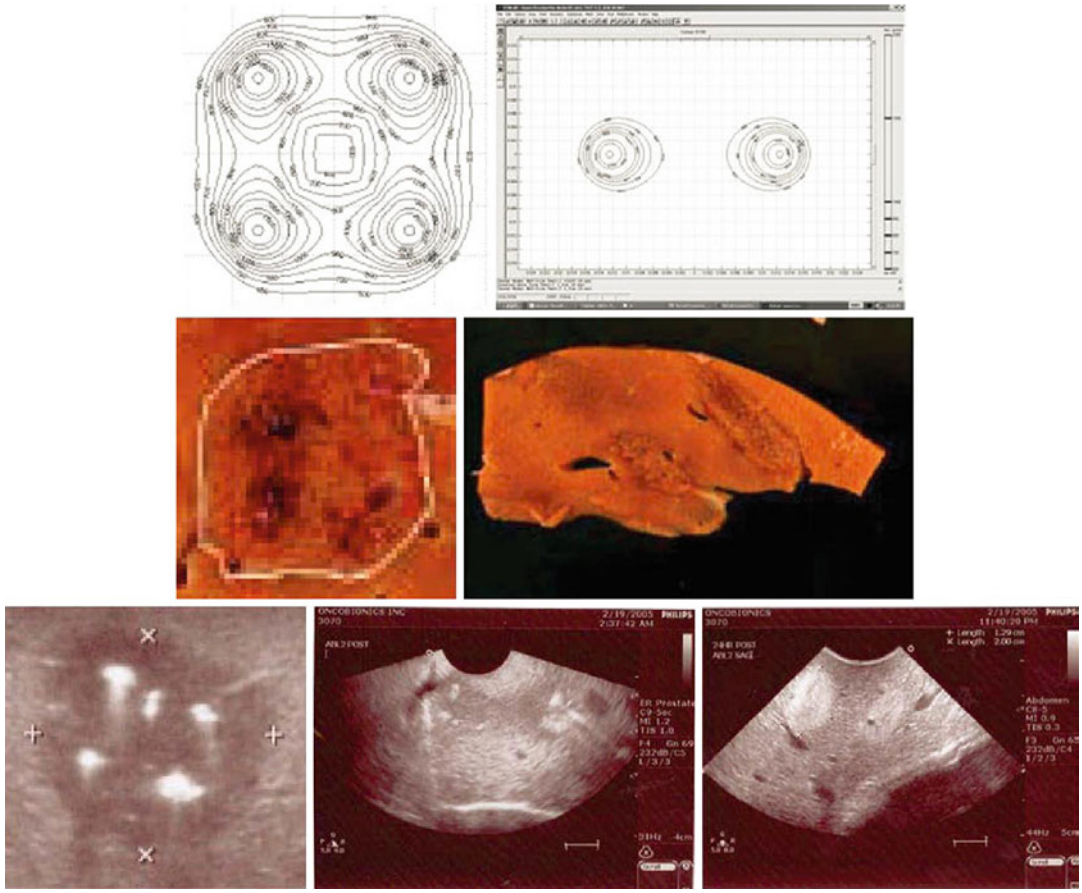

Fig. 2.10 Comparison between: *top* mathematical prediction of the extent of IRE ablation. *Outer* isoline is for 600 V/Cm, and each increment is 100 V/Cm. *Middle* is gross histology of the ablated area 24 h past ablation. *Bottom* is ultrasound images. The first column deals with the four electroporation probes case. For scale comparison, use the distance between the electroporation probes, which is 1.5 cm. The *right part* of the figure deals with a two-needle electroporation case in which the needles are separated by 2.5 cm. The pulse parameters are the same as in the left-hand case. Here, the ultrasound images show *left* ultrasound immediately after electroporation and *right* ultrasound immediately prior to necropsies. For scale compare the distance between electrodes which is 2.5 cm (From Ref. [21] with permission)

different IRE parameters after gadopentetate dimeglumine administration. Controls underwent IRE ablation without prior gadopentetate dimeglumine. MR imaging measurements (with conventional T1-weighted GRE and IR-prepared GRE methods) were performed 2 h after IRE to assess the IRE ablation zones, which were correlated with pathology-confirmed necrosis areas 24 h after IRE. The analysis shows that necrotic areas measured on the pathology images were well correlated with the hyperintense regions measured on T1-weighted GRE images and normal tissue-nulled IR images. Pathology measurements were also well correlated with the smaller hyperintense regions measured on those IR images with inversion times specifically selected to null signal from the peripheral penumbra surrounding the ablation zone. Bland-Altman plots indicated that these penumbra-nulled IR images provided more accurate predictions of IRE ablation zones, with T1-weighted GRE measurements tending to overestimate ablation zone sizes.

Electroporation is a complex biophysical process that occurs first at the nanoscale and within

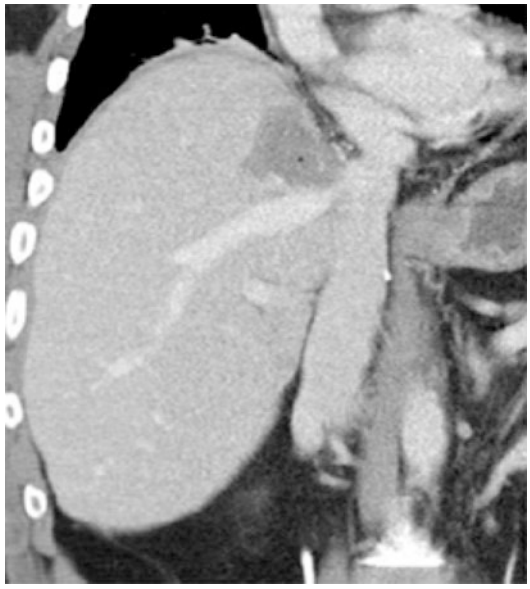

Fig. 2.11 CT image of post-IRE treatment (*dark area*) of a colorectal carcinoma near right atrium, diaphragm, and hepatic vein IVC confluence. Successful procedure without damage to these structures and no post-procedure pain (From Ref. [39] with permission)

microseconds. Therefore, while conventional medical imaging seems to produce a signature of the process of electroporation, it would be beneficial to develop a fundamental understanding of what the various imaging modalities show.

The potato, which has been long used as a model system for studying electroporation, is a good first model to study on the fundamentals of MRI of electroporation of cells, without systemic effects. When IRE is performed on a potato, the intracellular milieu containing melanin compounds is released and upon oxidation produces a visible dark area of the treated region (Fig. 2.12).

Our original choice of the MRI sequences was based on the assumption that the primary effect is related to the IRE damage to the cellular membrane and to the consequent release of intracellular content. It was anticipated that the main changes on MRI would be related to disruption of the cell membrane and a possible change in the signal from the phospholipids that form the cell membrane or from chemical changes due to the release of the intracellular contents – such as that related to the release of intracellular iron compounds and the eventual formation of melanin. To this end, we chose sequences that assume that NTIRE caused cell membrane chemical composition-related relaxation effects, i.e., shortening of relaxation times T1 and T2 [46]. Therefore, we used conventional spin echo, T1- and T2-weighted, FLAIR MRI sequences. To determine if the signal comes from phospholipids (lipid bilayer) or molecules with lipid like T1, we used a STIR sequence. STIR is used to eliminate signal from lipid or molecules with a T1 similar to that of lipid. The MRI acquisition parameters used in this study are listed as follows:

TE 19 ms, BW 10.4 kHz, TR 350 ms, NSA 3, matrix 192 × 256 for SE T1W images;

TE 125 ms, BW 20.8 kHz, TR 3,500 ms, NSA 3, matrix 256 × 256, for FSE T2W images;

TI 1800, TE 96 ms, BW 20.8, TR 8,000 ms, NSA 1, matrix 256 × 256 for FLAIR images; and

TI 225150 ms, TE 10.5 ms, BW 25, TR 2,800 ms, NSA 2, matrix 192 × 256 for STIR images (for all sequences, a 20-cm FOV, 3-mm slice thickness, and no gap were used). The results have shown that the MRI signals are lost from the electroporated region in imaging with the STIR sequence which is a special case of the inversion recovery-spin echo (IR-SE) pulse sequence. In this sequence, TI is chosen to have such a value that the signal from lipid or any tissue with T1 similar to lipid is suppressed. In contrast, strong signals were seen in the treated area on T1 and FLAIR sequences. Because any bright image in the ROI (region of interest) is lost in STIR-MRI, and strong signals are seen on T1 and FLAIR in the ROI, they could be caused by either lipids released from the cell membrane or by a molecule with T1 similar to that of lipid, released from the interior of the cell following disruption of the cell membrane. Regardless of the mechanism involved in the imaging process, it is obvious that MRI has the potential to produce images related to cell membrane disruption induced by NTIRE.

Electrical impedance tomography (EIT) is another imaging modality that has the potential to produce an image of the process of electroporation that is related to the cell membrane disruption due

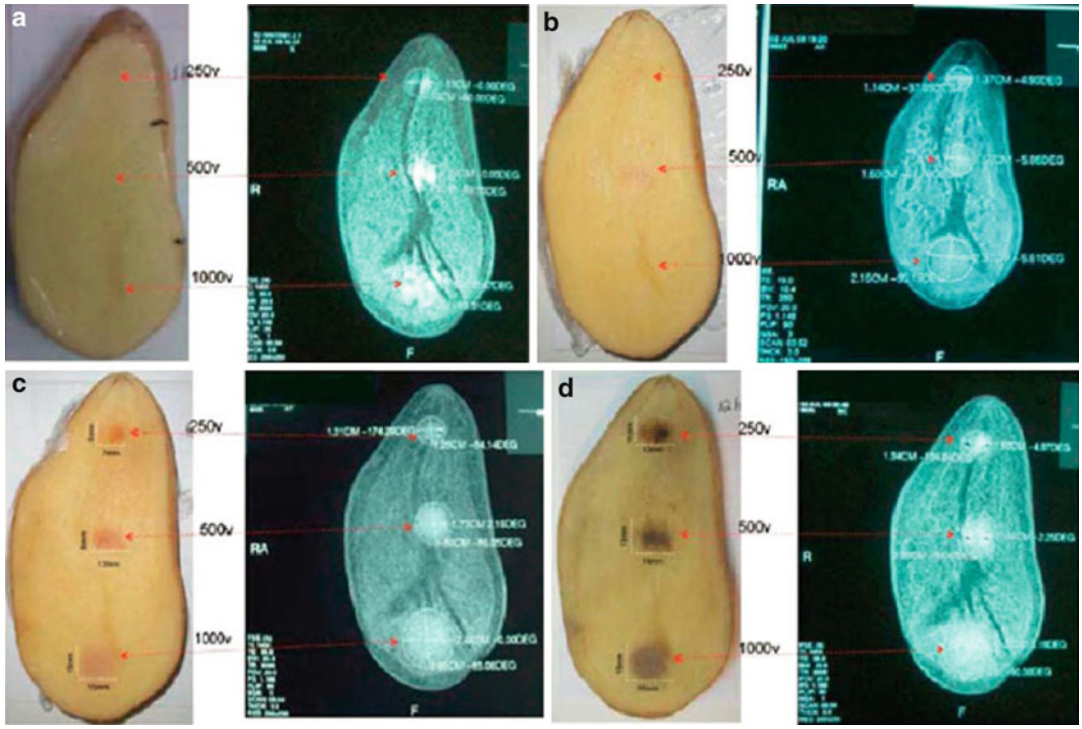

Fig. 2.12 Comparison between photographic images of the IRE-treated potato (*left*) and FLAIR-MRIs (*right*). The voltage used for electroporation is listed. The affected region is *dark* on the photographs due to oxidation and *bright* on the MRI due to either the signals from the lipids or some intracellular components. The dimensions of the affected areas are listed on the images. Times after IRE: (**a**) 1 h, (**b**) 3 h, (**c**) 6 h, (**d**) 12 h

to IRE. EIT produces a map of the tissue impedance. In an EIT implementation, electrodes are placed around the tissue, and very small currents are injected into the tissue while the voltage on the tissue boundary is measured [47]. Using the finite elements method, the impedance of the entire tissue is modeled, and a solution for the most likely configuration that fits the problem is obtained [48]. EIT is known as a suitable technique for imaging fast dynamic phenomena in three dimensions [49]. While IRE can produce various biophysical phenomena, the first event of importance is the permeabilization of the cell membrane. We have shown that the permeabilization of the cell membrane by electroporation produces a change in the electrical impedance of the cell because it provides a new path for ionic currents [50]. Therefore, we have suggested and demonstrated that EIT can produce an instantaneous image of the cell membrane permeabilization [51].

Summary

The goal of this brief review was to introduce the new minimally invasive tissue ablation modality of nonthermal irreversible electroporation and various important aspects related to the clinical use of this modality. NTIRE has several unique attributes that do not exist in other tissue ablation modalities; it can ablate large volumes of tissue rapidly, and it affects only the cell membrane. While this is very promising, substantial further research is needed to take full advantage of the special attributes of the technique. Among them are developing a fundamental understanding of the biophysics of the process, developing advanced treatment planning mathematical algorithms, and developing medical-imaging technologies optimized for NTIRE.

Cross-References

- Anesthesia Challenges in Interventional Oncology
- Cryoablation
- Devices and Equipment in Interventional Oncology and Their Operation
- Emerging Technologies in the Treatment of Cancer
- Image-Guided High-Intensity Focused Ultrasound in the Treatment of Cancer
- Imaging of Interventional Therapies in Oncology: Computed Tomography
- Imaging of Interventional Therapies in Oncology: Magnetic Resonance Imaging
- Imaging of Interventional Therapies in Oncology: Positron Emission Tomography/Computed Tomography
- Imaging of Interventional Therapies in Oncology: Ultrasound
- Microwave Ablation for Cancer: Physics, Performance, Innovation, and the Future
- Tumor Ablation: An Evolving Technology

References

1. Weaver J, Chizmadzhev YA. Theory of electroporation: a review. Bioelectrochem Bioenerg. 1996;41:135–60.
2. Chen C, Smye SW, Robinson MP, Evans JA. Membrane electroporation theories: a review. Med Biol Eng Comput. 2006;44:5–14.
3. Stopper H, Zimmermann U, Wecker E. High yields of DNA-transfer into mouse L cells by electropermeabilization. Z Naturforsch C. 1985;40:929–32.
4. Teissie J, Golzio M, Rols MP. Mechanisms of cell membrane electropermeabilization: a minireview of our present (lack of?) knowledge. Biochim Biophys Acta. 2005;1724:270–80.
5. Neumann E, Schaeffer-Ridder M, Wany Y, Hofschneider PH. Gene transfer into mouse lymphoma cells by electroporation in high electric fields. EMBO J. 1982;1:841–5.
6. Rubinsky B. Irreversible electroporation in medicine. Technol Cancer Res Treat. 2007;6(4):255–60.
7. Lelieveld HLM, Netermans S, de Haan SWH, editors. Food preservation by pulsed electric fields. From research to applications. Cambridge: Woodhead; 2007.
8. Beebe SJ, Fox PM, Rec LJ, Somers K, Stark RH, Schoenbach KH. Nanosecond pulsed electric field (nsPEF) effects on cells and tissues: apoptosis induction and tumor growth inhibition. IEEE Trans Plasma Sci. 2002;30:286–92.
9. Hamilton WA, Sale AJH. Effects of high electric fields on microorganisms. 2. Mechanism of action of the lethal effect. Biochim Biophys Acta. 1967;148:789–800.
10. Sale AJ, Hamilton WA. Effects of high electric fields on microorganisms. 1. Killing of bacteria and yeasts. Biochim Biophys Acta. 1967;148:781–8.
11. Sale AJ, Hamilton WA. Effects of high electric fields on microorganisms. 3. Lysis of erythrocytes and protoplasts. Biochim Biophys Acta. 1968;163:37–43.
12. Rubinsky B, editor. Irreversible electroporation, Series in biomedical engineering. New York: Springer; 2010. p. 314.
13. Davalos RV, Mir L, Rubinsky B. Tissue ablation with irreversible electroporation. Ann Biomed Eng. 2005;33(2):223–31.
14. Davalos RV, Rubinsky B. Temperature considerations during irreversible electroporation. Int J Heat Mass Transfer. 2008;51(23–24):5617–22.
15. Bower M, Sherwood L, Li Y, Martin R. Irreversible electroporation of the pancreas: definitive local therapy without systemic effects. J Surg Oncol. 2011;104(1):22–8.
16. Charpentier KP, Wolf F, Noble L, Winn B, Resnick M, Dupuy DE. Irreversible electroporation of the pancreas in swine: a pilot study. HPB. 2010;12(5):348–51.
17. Ball C, Thomson K, Kavnoudias H. Irreversible electroporation: a new challenge in "out of operating theater" anesthesia. Anesth Analg. 2010;110:1305–9.
18. Lee EW, Chen C, Prieto VE, Dry SM, Loh CT, Kee ST. Advanced hepatic ablation technique for creating complete cell death: irreversible electroporation. Radiology. 2010;255(2):426–33.
19. Thomson KR, Cheung W, Ellis SJ, Federman D, Kavnoudias H, Loader-Oliver D, Roberts S, Evans P, Ball C, Haydon A. Investigation of the safety of irreversible electroporation in humans. J Vasc Interv Radiol. 2011;22(5):611–21.
20. Tracy CR, Kabbani W, Cadeddu JA. Irreversible electroporation (IRE): a novel method for renal tissue ablation. BJU Int. 2011;107(12):1982–7.
21. Rubinsky B, Onik G, Mikus P. Irreversible electroporation: a new ablation modality–clinical implications. Technol Cancer Res Treat. 2007;6(1):37–48.
22. Onik G, Mikus P, Rubinsky B. Irreversible electroporation: implications for prostate ablation. Technol Cancer Res Treat. 2007;6(4):295–300.
23. Schoellnast H, Monette S, Ezell PC, Deodhar A, Maybody M, Erinjeri JP, Stubblefield MD, Single GW, Hamilton WC, Solomon SB. Acute and subacute effects of irreversible electroporation on nerves: experimental study in a pig. Radiology. 2011;260(2):421–7.
24. Li W, Fan QY, Ji ZW, Qiu X, Li Z. The effects of irreversible electroporation (IRE) on nerves. PLoS One. 2011;6(4):e18831. doi:10.1371/journal.pone.0018831.
25. Maor E, Ivorra A, Leor J, Rubinsky B. Irreversible electroporation attenuates neointimal formation after

angioplasty. IEEE Trans Biomed Eng. 2008;55(9): 2268–74.
26. Maor E, Ivorra A, Rubinsky B. Non thermal irreversible electroporation: novel technology for vascular smooth muscle cells ablation. PLoS One. 2009;4(3): e4757.
27. Neal RE, Singh R, Hatcher HC, Kock ND, Torti SV, Davalos RV. Treatment of breast cancer through the application of irreversible electroporation using a novel minimally invasive single needle electrode. Breast Cancer Res Treat. 2010;123(1):295–301.
28. Brausi M, Gilberto GL, Simonini GL, Botticelli L, Gregorio C. Irreversible electroporation, a novel technology for focal ablation of prostate cancer: results of an interim pilot safety study in low-risk patients. Anticancer Res. 2011;31(5):1834–5.
29. Becker SM, Kuznetsov AV. Thermal damage reduction associated with in vivo skin electroporation: a numerical investigation justifying aggressive precooling. Int J Heat Mass Transfer. 2007;50:105–16.
30. Daniels CR, Rubinsky B. Electrical field and temperature model of nonthermal irreversible electroporation in heterogeneous tissues. J Biomech Eng. 2009; 131(7):071006.
31. Edd JF, Horowitz L, Davalos RV, Mir LM, Rubinsky B. In vivo results of a new focal tissue ablation technique: irreversible electroporation. IEEE Trans Biomed Eng. 2006;53(7):1409–15.
32. Edd JF, Davalos RV. Mathematical modeling of irreversible electroporation for treatment planning. Technol Cancer Res Treat. 2007;6:275–86.
33. Somersalo E, Cheney M, Isaacson D. Existence and uniqueness for electrode models for electric current computed tomography. SIAM J Appl Math. 1992; 52:1023–40.
34. Pennes HH. Analysis of tissue and arterial blood temperatures in the resting forearm. J Appl Physiol. 1948;1:93–122.
35. Rubinsky B. Numerical bio-heat transfer. In: Minkowycz WJ, Sparrow EM, Murthy JY, editors. John Wiley ed. Handbook of numerical heat transfer. 2nd ed. Hoboken, NJ: Wiley; 2006, p. 851–93.
36. Henriques FC, Moritz AR. Studies in thermal injuries: the predictability and the significance of thermally induced rate processes leading to irreversible epidermal damage. Arch Pathol. 1947;43:489–502.
37. Diller KR. Modeling of bioheat transfer processes at high and low temperatures. In: Choi YI, editor. Bioengineering heat transfer. Boston: Academic; 1992. p. 157–357.
38. Onik G, Rubinsky B. Irreversible electroporation: first patient experience focal therapy of prostate cancer. In: Rubinsky B, editor. Irreversible electroporation, Series in biomedical engineering. Berlin: Springer; 2010.
39. Thomson K. Human experience with irreversible electroporation. In: Rubinsky B, editor. Irreversible electroporation, Series in biomedical engineering. Berlin: Springer; 2010.
40. Rossmeisl JH, Garcia PA, Lanz OI, Hena-Guerrero N, Davalos VR. Successful treatment of a large soft tissue sarcoma with irreversible electroporation. J Clin Oncol. 2011;29(13):E372–7.
41. Onik CC, Goldenberg HI, Moss AA, Rubinsky B, Christianson M. Ultrasonic characteristics of frozen liver. Cryobiology. 1984;21:321–8.
42. Gilbert JC, Onik GH, Haddick WK, Rubinsky B. The use of ultrasonic imaging for monitoring cryosurgery. IEEE Trans Biomed Eng. 1984;8:563.
43. Lee EW, Loh CT, Kee ST. Imaging guided percutaneous irreversible electroporation: ultrasound and immunohistological correlation. Technol Cancer Res Treat. 2007;6(4):287–94.
44. Zhang Y, Guo Y, Ragin AB, Lewandowski RJ, Yang GY, Nijm GM, Sahakian AV, Yang GY, Omary RA, Larson AC. MR imaging to assess immediate response to irreversible electroporation for targeted ablation of liver tissue: preclinical feasibility studies in a rodent model. Radiology. 2010;256(2): 424–32.
45. Guo Y, Zhang Y, Nijm GM, Shakian AV, Yang GY, Omary RA, Larson AC. Irreversible electroporation in the liver: contrast inversion imaging approaches to differentiate reversible electroporation penumbra from irreversible electroporation zones. Radiology. 2011;258(2):461–8.
46. Hjouj M, Rubinsky B. Magnetic resonance imaging characteristics of non-thermal irreversible electroporation in vegetable tissue. J Membr Biol. 2010; 236(1):137–46.
47. Jossinet J, Marry E, Matias A. Electrical impedance endotomography. Phys Med Biol. 2002;47:2189–202.
48. Lionheart WR. EIT reconstruction algorithms: pitfalls, challenges and recent developments. Physiol Meas. 2004;25:125–42.
49. Metherall P, Barber DC, Smallwood RH, Brown BH. Three-dimensional electrical impedance tomography. Nature. 1996;380:509–12.
50. Huang Y, Rubinsky B. Micro-electroporation: improving the efficiency and understanding of electrical permeabilization of cells. Biomed Microdevices. 1999;2(2):145–50.
51. Granot Y, Ivorra A, Maor E, Rubinsky B. In vivo imaging of irreversible electroporation by means of electrical impedance tomography. Phys Med Biol. 2009;54(16):4927–43.